Engineering Science and Technology, an International Journal 19 (2016) 1731–1741

HOSTED BY

Contents lists available at ScienceDirect

Engineering Science and Technology, an International Journal

journal homepage: www.elsevier.com/locate/jestch

Invited Full Length Article

A solar PV water pumping solution using a three-level cascaded inverter connected induction motor drive

Ramulu Chinthamalla [a], Sanjeevikumar Padmanaban [b,c,*], Ramsha Karampuri [a], Sachin Jain [a], Ahmet H. Ertas [d], Viliam Fedak [e]

[a] Department of Electrical Engineering, National Institute of Technology, Warangal (T.S.), India
[b] Department of Electrical and Electronics Engineering, University of Johannesburg, Auckland Park, South Africa
[c] Research and Development, Power Electronics Division, Ohm Technologies, Chennai, India
[d] Department of Biomedical Engineering, Faculty of Engineering, Karabuk University, Karabuk, Turkey
[e] Department of Electrical Engineering & Mechatronics, Technical University of Kosice, Slovakia

ARTICLE INFO

Article history:
Received 12 August 2016
Revised 26 August 2016
Accepted 28 August 2016
Available online 8 September 2016

Keywords:
Centrifugal pump
Maximum Power Point Tracking
PhotoVoltaic
Space Vector Pulse Width Modulation
Three-level inversion

ABSTRACT

This paper presents a single-stage solution for PV fed three-phase induction motor (IM) water pumping system. The given solution uses time tested, two two-level cascaded H-bridge inverters to give three-level voltage output to the IM pump drive. The proposed system is operated using the control strategy which includes Maximum Power Point Tracking (MPPT), Space Vector Pulse Width Modulation (SVPWM) and V/*f* control. The MPPT algorithm generates the modulation index 'm_a' which is used to operate the cascaded inverter and generates three-level output voltage under all environmental conditions. This helps in improving the THD of IM phase current, thereby reducing the torque ripple. In addition, the 'm_a' value is used to define the IM operating frequency. This helps in further improvement in the IM performance. All the details of the proposed system regarding the system modeling along with simulation and experiment results are given in the manuscript. In addition, the comparison of the propsoed solution with the conventional system i.e., two-level inverter connected PV pumping system is presented.

1. Introduction

There is a sharp increasing demand for electrical energy, due to the modernization of the society requirements and its increasing applications in industrial and domestic needs. One solution to meet the growing power demand could be to increase the generating capacity of central power plant. This is restricted by environmental and ecology constraints. Other good solution would be the use of non-conventional or renewable sources like wind, PV, fuel cell etc. Among the existing non-conventional sources of energy, solar PhotoVoltaic (PV) technology is more popular as it has many advantages as described in various literature [1–4]. The benefits of solar PV systems are: it absorbs the ever-lasting solar energy at free of cost, eco-friendly without generating any kind of pollution in the atmosphere, and offers noise less operation and low maintenance when compared with the other non-conventional energy sources.

The solar PV array directly converts the solar energy from the Sun into dc electric power. The generated dc power from the PV array is conditioned or transformed into the required form using Power Conditioning Unit (PCU). The PCU can be any inverter or converter circuit depending on the application of the PV system. With respect to the application, solar PV system can be broadly divided into two categories: (i) Grid connected PV system and (ii) Stand-alone PV system. In grid connected PV systems [5–7], the solar PV power is fed into the grid in the form of high quality sinusoidal current using higher or multilevel inverter [8,9]. Whereas, in stand-alone PV system solar PV source with or without additional sources maintains the defined voltage and current required by the stand-alone loads [10–12]. Additional sources can be battery, wind power, fuel cell etc., and they are required due to uncertainty in the PV power generation. However, stand-alone applications like solar water pump used in agriculture, multi-storey buildings or industries etc., with water tank-storage may not require additional sources. Also, in such systems PV source can always be operated near maximum power point (MPP) which gives the option of using

* Corresponding author at: Department of Electrical and Electronics Engineering, University of Johannesburg, Auckland Park, South Africa.
E-mail address: sanjeevi_12@yahoo.co.in (P. Sanjeevikumar).
Peer review under responsibility of Karabuk University.

http://dx.doi.org/10.1016/j.jestch.2016.08.019
2215-0986/

generated PV power efficiently. Some good solutions given in the literature for the PV fed water pump drive systems briefed below.

Some of the initial solutions for PV pumping system includes, the use of dc motor without PCU [13,14] and with a PCU [15–17]. However, because of the high cost and continuous maintenance of dc motors, the later solutions were proposed using an induction motor (IM) [18–22]. The solutions given in [18–22] employs two PCUs, one (dc-dc converter) for extracting maximum power from PV source and the other (dc-ac inverter) is to control the motor-pump. The second PCU i.e., dc-ac inverter used in [18–22] is a two-level three-phase H-bridge inverter. So, more number of PCUs and two-level output increases the losses and ripple content in the motor current of the PV system respectively. Therefore, there is the requirement of single-stage power conditioning (i.e., single PCU) solution for PV pumping system with more than two-level voltage output because of its advantages given in [23–25] and the system is shown in Fig. 1.

One such solution based on the Neutral Point Clamped (NPC) inverter configuration has been proposed in [26]. The proposed solution is good, as it involves single PCU with three-level inverter output voltage. However, the proposed system [26] uses complicated variable step MPPT tracking which gives reference speed as an output. Further, the number of switching devices used are more resulting in higher cost and weight. Recently, another solution using single PCU and three-level inversion has been presented in [27,28]. The PV pumping solutions given in [27,28] uses an open-end winding induction motor connected to two two-level inverters on both the ends of the stator winding. These solutions are advantageous over the system given in [26], because of the use of simple control technique, less cost and better fault-tolerance. However, the use of open-end winding induction motor suffers with the requirement of more number of wires (cables between motor and inverter output) and the other disadvantages mentioned in [29]. In addition, the open-end winding induction motors are not commercially available in the market. Therefore, a simple solution using commercially available 3-Φ induction motor would be good one.

Thus, from the above discussion, it is evident that there is requirement of low cost single-stage three-level PV pumping system with simple control which integrates both MPPT and motor control. This paper gives a solution in which the value of modulation index 'm_a' controls the PV source power. Further, the calculated value of 'm_a' is again used by V/f control for defining the fundamental frequency and magnitude of the phase voltage applied to the motor. Usage of V/f control with pump or fan type application further helps in the efficient or optimized operation of a three-phase motor. Thus, the proposed system effectively uses the PV source and controls the motor efficiently.

Rest of the manuscript is divided into six-sections: working principle and modeling of the proposed system are presented in Section 2. Section 3 describes the control strategy and MPPT algorithm used for the proposed system. Section 4 gives the simulation results showing the performance of the proposed system. Section 5 gives the comparison of the proposed PV pumping system with the conventional two-level PV pumping system. Section 6 gives the experimental results to support the simulation results. And the last section describes the conclusion of the paper.

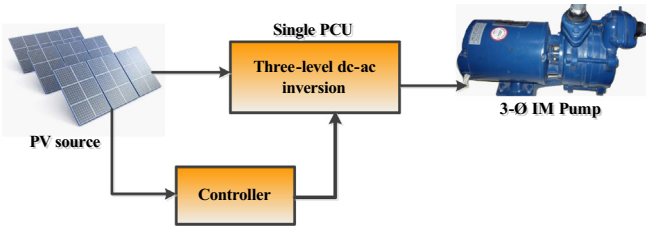

Fig. 1. Proposed single-stage PV powered three-level inverter connected to three-phase induction motor-pump.

2. Working principle and modeling of the proposed system

The circuit schematic diagram of the proposed PV source fed three-level cascaded inverter connected to an induction motor coupled a centrifugal pump load is shown in Fig. 2. The proposed system consists of solar PV array, three-level cascaded inverter (with Inverter-1 and Inverter-2 which are conventional two-level inverters connected in cascaded manner) [30], three-phase star-connected squirrel cage induction motor, centrifugal pump load and a dSPACE controller. Power generated by the PV source is conditioned in the required form by three-level cascaded inverter and is transferred to motor pump load. To analyze the performance of the proposed PV pumping system, a simulation model is developed by combining the individual models as discussed below.

2.1. PV source model

PV source model is developed using basic unit model of a PV cell. The electrical equivalent current–voltage characteristics for the PV array using basic cell [31] equation is given by:

$$i_{pv} = N_p\left\{i_{sc} - i_s\left[e^{\frac{q(v_{pv})}{N_s\eta kT}} - 1\right]\right\} \tag{1}$$

In Eq. (1) i_{pv}, i_{sc}, i_s are the PV array current (A), the short-circuit current of PV cell (A), and the reverse saturation current of diode (A) respectively. The short-circuit current depends on the Sun insolation (G) and the temperature (T). N_p and N_s are the number of parallel and series connected PV cells respectively, η is the diode ideality factor, k is the boltzmann constant, q is the electron charge, T is the array operating temperature in kelvin and v_{pv} is the PV array voltage (V). In simulation the PV array voltage (v_{pv}), insolation (Suns) and the temperature (°C) are taken as inputs for the calculation of PV array current as given in Eq. (1) (see Fig. 3). And the output terminals of PV array are connected to three-level cascaded inverter via buffer capacitors C_{pv1} and C_{pv2} as indicated in Fig. 2. Applying KCL at terminal nodes '$c1$' & '$c2$' of buffer capacitors (Fig. 2),

$$i_{pv} = i_{Cpv1} + i_{inv1} = C_{pv1}\frac{dv_{Cpv1}}{dt} + i_{inv1} \tag{2}$$

$$i_{Cpv1} = i_{Cpv2} + i_{inv2} = C_{pv2}\frac{dv_{Cpv2}}{dt} + i_{inv2} \tag{3}$$

where v_{Cpv1} and i_{Cpv1} are the voltage across and current through the capacitor C_{pv1}; v_{Cpv2} and i_{Cpv2} are the voltage across and current through the capacitor C_{pv2}; i_{inv1} and i_{inv2} are the currents drawn by Inverter-1 and Inverter-2 respectively. Integral solution for Eqs. (2) and (3) give dc-bus capacitor voltage v_{Cpv1} and v_{Cpv2}. The dc-bus capacitor voltages are added to form PV voltage, v_{pv} which is given back to PV source model as an input as shown in Fig. 3.

2.2. Mathematical model of three-level cascaded inverter

Mathematical model of the three-level cascaded inverter is developed using switching function equations [27]. A switching logic S_{XY} (where $X \in \{r, y, b\}$ and $Y \in \{1, 2\}$) is adopted to model the inverter for the proposed system. The switching function S_{XY} has value '1' or '0' represents top switch corresponding to phase 'X'of inverter 'Y' is turned 'ON' or 'OFF' respectively. The cascaded inverter comprises of six poles ($r1$, $y1$, $b1$, $r2$, $y2$ and $b2$) and 12 switches (four switches per phase-leg). The considered inverter

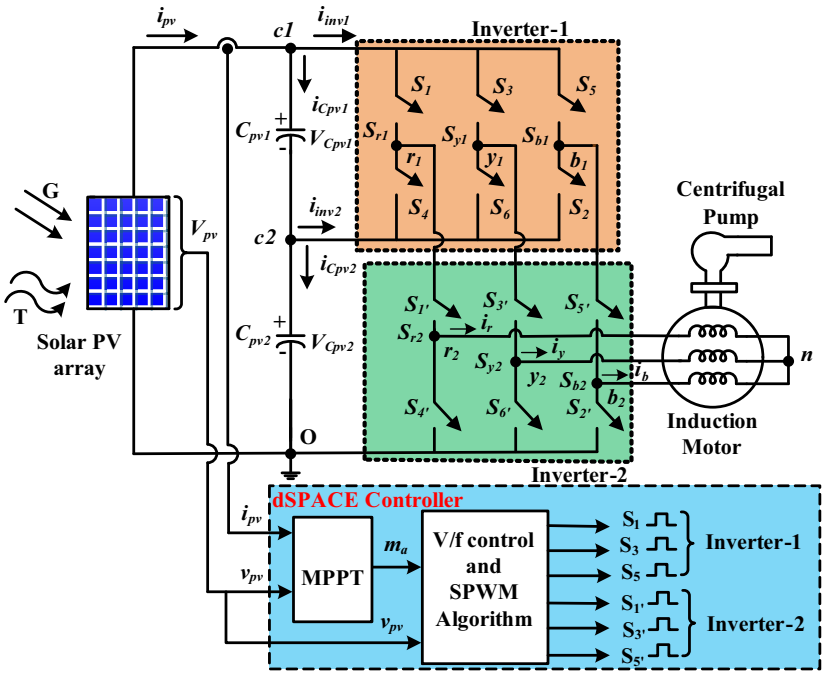

Fig. 2. Schematic circuit diagram of the proposed single-stage PV powered three-level cascaded inverter with induction motor-pump.

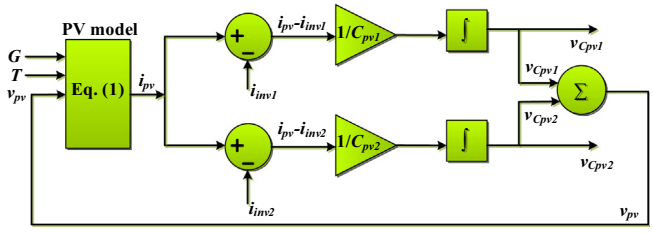

Fig. 3. Mathematical model of PV module.

configuration produces three-levels in the pole-voltage, which are $V_{Cpv1}+V_{Cpv2}$, V_{Cpv2}, and 0. The pole-voltage is calculated with respect to dc neutral nodal point 'O' (see Fig. 2). The voltage 'v_{XYo}' represents the pole-voltage for '*X*' leg of inverter '*Y*'. It can be calculated using the switching function and dc-bus voltage (V_{Cpv1}) and (V_{Cpv2}) across the capacitors C_{pv1} and C_{pv2} respectively. Thus, the pole-voltage for '*r*' phase of Inverter-1 'v_{r1o}' is given as,

$$v_{r1o} = S_{r1} \times (V_{Cpv1} + V_{Cpv2}) + \bar{S}_{r1} \times V_{Cpv2} \tag{4}$$

where ' – ' represents complementary value of switching function i.e., its value is '0' or '1' for the top switch of corresponding leg is turned 'ON' or 'OFF' respectively. Similarly, pole-voltage 'v_{y1o}' and 'v_{b1o}' of other phases '*y*' & '*b*' respectively for Inverter-1 are given as,

$$v_{y1o} = S_{y1} \times (V_{Cpv1} + V_{Cpv2}) + \bar{S}_{y1} \times (V_{Cpv2}) \tag{5}$$

$$v_{b1o} = S_{b1} \times (V_{Cpv1} + V_{Cpv2}) + \bar{S}_{b1} \times (V_{Cpv2}) \tag{6}$$

Using the same strategy, the pole-voltages 'v_{r2o}', 'v_{y2o}' and 'v_{b2o}' of '*r*', '*y*' and '*b*' phases for Inverter-2 are given as,

$$v_{r2o} = S_{r1}S_{r2} \times (V_{Cpv1} + V_{Cpv2}) + \bar{S}_{r1}S_{r2}(V_{Cpv2}) \tag{7}$$

$$v_{y2o} = S_{y1}S_{y2} \times (V_{Cpv1} + V_{Cpv2}) + \bar{S}_{y1}S_{y2}(V_{Cpv2}) \tag{8}$$

$$v_{b2o} = S_{b1}S_{b2} \times (V_{Cpv1} + V_{Cpv2}) + \bar{S}_{b1}S_{b2}(V_{Cpv2}) \tag{9}$$

Thus, the common mode voltage 'v_{no}' can be determined as (from Fig. 2),

$$v_{no} = \frac{1}{3}(v_{r2o} + v_{y2o} + v_{b2o}) \tag{10}$$

where '*n*' is the machine stator winding neutral point. Once the common mode voltage is known, the motor phase voltage at cascaded inverter output is given by,

$$v_{r2n} = v_{r2o} - v_{no} \tag{11}$$

where 'v_{r2n}' is the motor *r*-phase voltage. Similarly, other phase voltages 'v_{y2n}' and 'v_{b2n}' can be derived. Now, once the phase voltage for the motor is known, then the respective phase current can be derived using IM model as described in the next section. The derived phase current can further be utilized in the calculation of current through Inverter-1 'i_{inv1}' and Inverter-2 'i_{inv2}' as given below.

$$i_{inv1} = S_{r1}S_{r2}i_r + S_{y1}S_{y2}i_y + S_{b1}S_{b2}i_b \tag{12}$$

$$i_{inv2} = \bar{S}_{r1}S_{r2}i_r + \bar{S}_{y1}S_{y2}i_y + \bar{S}_{b1}S_{b2}i_b \tag{13}$$

2.3. Modeling of three-phase IM coupled with centrifugal pump load

The derived three-phase output voltages (v_{r2n}, v_{y2n} and v_{b2n}) of the cascaded inverter are applied to the stator winding of IM after transforming them to synchronously rotating reference frame as presented in [32]. The applied voltages are responsible to develop an electromagnetic torque in the IM. The dynamics of the mechanical torque developed by the IM coupled to a centrifugal pump can be expressed as,

$$m_d = J\frac{d\omega_r}{dt} + B\omega_r + K\omega_r^2 \tag{14}$$

where '*J*' is the moment of inertia (kg-m^2), 'ω_r' is the rotor angular speed (rps), '*B*' is friction coefficient and '*K*' is the centrifugal pump constant.

3. MPPT algorithm and control strategy

The above developed model of PV pumping system requires a better control strategy to analyze its performance. The proposed system employs an integrated control strategy which assimilates MPPT algorithm, V/*f* control and SVPWM technique. In the given solution, simple and robust '*P* & *O*' algorithm [33] is employed to extract maximum power from solar PV array. Whereas, the open-loop V/*f* control is chosen to improve the motor performance and the SVPWM technique is to operate the power semiconductor devices of the inverter with better dc-bus utilization.

The proposed control strategy is shown in Fig. 4. The control algorithm first initializes the value of modulation index 'm_a' to its minimum value 'm_{amin}'. The value of 'm_a' is used to calculate the fundamental frequency of the modulating signal 'f_{mod}' and the frequency of the carrier signal 'f_s' as given in Eqs. (15) and (16).

$$f_{\text{mod}} = \begin{cases} \frac{m_a \times 50}{0.866} & \text{for } m_a \leqslant 0.866 \\ 50 & \text{for } m_a > 0.866 \end{cases} \tag{15}$$

where, the rated frequency of the phase voltage/current of motor is 50 Hz and the boundary of linear modulation is 0.866 for the proposed PWM technique.

$$f_s = f_{\text{mod}} \times Samples \tag{16}$$

The time periods of the modulating ('T_{mod}') and the carrier signal ('T_s') are obtained by inverting Eqs. (15) and (16) respectively. The values of 'f_{mod}' and 'f_s' are calculated using 'm_a' and both are updated for every change in 'm_a'. This is done for two reasons: one is to maintain the synchronization between both the modulating and carrier signals and the other is to maintain the fixed number of samples per fundamental cycle. This gives the opportunity to operate the system with variable switching frequency [34]. The number of samples are calculated by the counter using the value of 'T_{mod}' as shown in Fig. 4. In this paper the number of samples per fundamental cycle are considered to be 48. Hence, the switching frequency in the propsoed system varies from 554 Hz (corresponding to $m_{amin} = 0.2$) to 2.4 kHz (corresponding to $m_a = 0.866$ i.e., boundary of linear modulation).

The MPPT algorithm uses the value of samples (i.e., 48 in this paper) to hold the logic/calculations until the counter counts up to 48 within a time period 'T_{mod}'. The logic/calculations for implementing the MPPT algorithm are incorporated inside the '*P* & *O*' MPPT algorithm block as shown in Fig. 4. The logic/calculations are held so as to provide enough time to update the values of PV voltage and current. In other words, this helps in improving the accuracy of the MPPT algorithm which is described below.

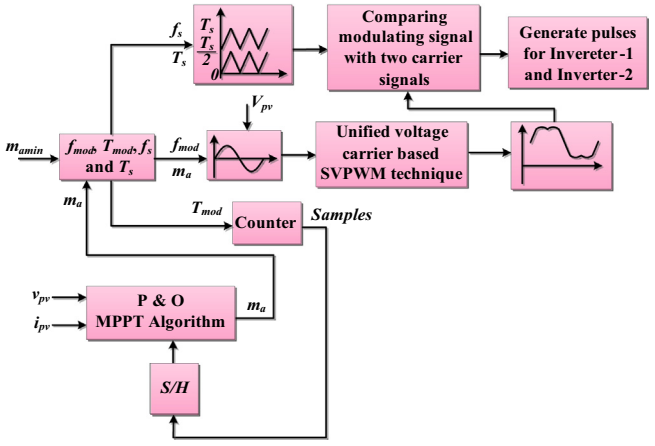

Fig. 4. The block diagram of the control strategy used for the proposed system.

The '*P* & *O*' MPPT algorithm senses the instantaneous PV voltage 'v_{pv}' and PV current 'i_{pv}'; then calculates PV power 'p_{pv}'. These values are averaged within a time period 'T_{mod}' and are stored as previous values $V_{pv}(n-1)$ and $P_{pv}(n-1)$. After one fundamental cycle i.e., 48 samples the present PV voltage $V_{pv}(n)$ and power $P_{pv}(n)$ are obtained by averaging the instantaneous values. These present values and previously obtained values are compared to determine the operating region in the *p-v* curve (see Fig. 5) as described in Eqs. (17) and (18).

$$\frac{P_{pv}(n) - P_{pv}(n-1)}{V_{pv}(n) - V_{pv}(n-1)} < 0 \quad \text{then} \quad m_a = m_a + \Delta m_a \tag{17}$$

$$\frac{P_{pv}(n) - P_{pv}(n-1)}{V_{pv}(n) - V_{pv}(n-1)} > 0 \quad \text{then} \quad m_a = m_a - \Delta m_a \tag{18}$$

Now, the updated value of 'm_a' from the MPPT algorithm is used to update the values of 'f_{mod}', 'f_s', 'T_{mod}', and 'T_s'. These values are used to generate the reference modulating signal with the magnitude '$m_a \times V_{pv}$' and frequency 'f_{mod}'. This is done to ensure the implementation of V/*f* control. Furthermore, two carrier signals are generated: one with the magnitude varying from '0 to $T_s/2$' and the other is with the magnitude varying from '$T_s/2$ to T_s' (see Fig. 4). Both the carrier signals are generated with a frequency 'f_s'.

The reference modulating signal is a sinusoidal waveform which is conditioned by using the unified voltage carrier based SVPWM technique [27]. This algorithm is described briefly in [27], which generates a modulating signal of camel-hump nature as shown in Figs. 4 and 6. The generated modulating signal is now compared with the two carrier signals as shown in Fig. 6. This is done for all the values of 'm_a', so as to obtain the three-level motor phase voltage output in entire linear modulation region (i.e., up to $m_a = 0.866$). The other reason to get three-level voltage in linear modulation region is because of the use of single PV source. Otherwise, with the two electrically isolated PV sources one can obtain two-level and three-level voltages for different ranges of 'm_a' [27]. The gating signals required by the inverter switches are generated by comparing the modulation and the carrier signals as shown in Figs. 4 and 6.

4. Simulation results and analysis

To analyze and verify the performance, the proposed system (as shown in Fig. 2) is simulated by using MATLAB/Simulink software. The specifications used for solar PV array and 3-Φ IM are furnished in Table 1. The proposed system is simulated for various environmental conditions with increasing and decreasing trend for insolation (G) and ambient temperature (T) as shown in subplot (a) of Fig. 7. The values of G and T considered for simulation are: from

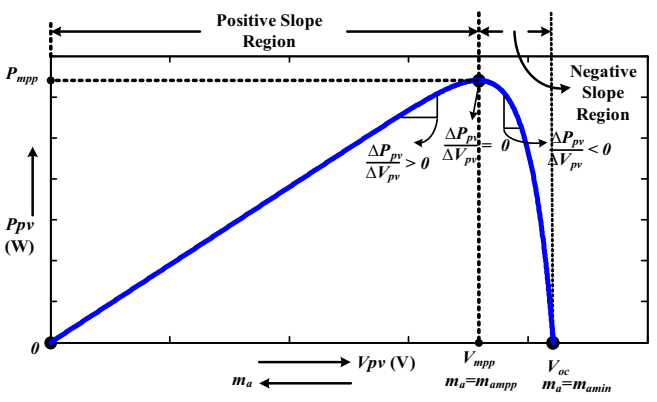

Fig. 5. The *p-v* characteristics of a PV module.

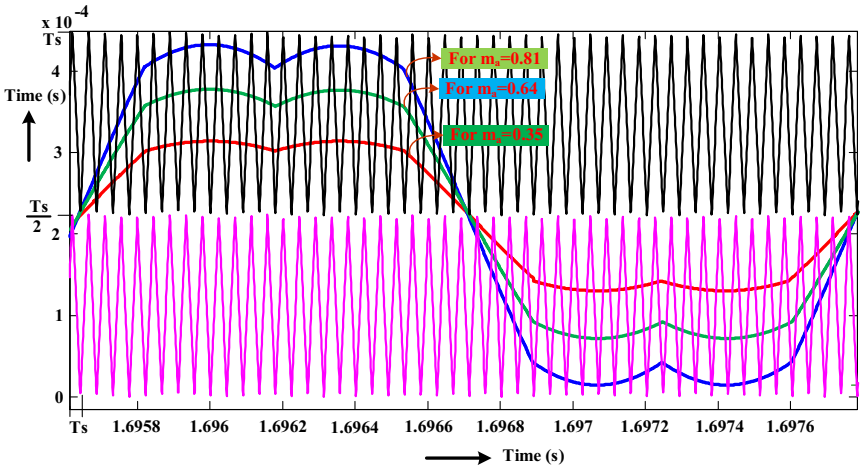

Fig. 6. Modulating signal comparison with the carrier signal for different values of modulation index, 'm_a'.

Table 1
Specifications and parameters of solar PV module and 3-Φ IM respectively.

Parameter	Value	Parameter	Value
PV module @ STC (1 Sun, 25 °C) parameters [31]			
Open-circuit voltage, V_{oc}	21.0 V	Current at MPP, I_{MPP}	3.5 A
Short-circuit current, I_{sc}	3.74 A	Power at MPP, P_{MPP}	59.9 W
Voltage at MPP, V_{MPP}	17.1 V	PV array size	33 × 2
Induction motor parameters			
Rated voltage (L-L)	400 V	Supply frequency, f	50 Hz
Rated speed, N_r	1430 rpm	No. of poles, p	4
Stator winding resistance, r_s	1.405 Ω	Rotor winding resistance, r_r	1.395 Ω
Leakage reactance, $x_{ls} = x_{lr}$	1.8344 Ω	Rated power	4 kW

time 0 to 8 s, G = 0.1 Suns and T = 25 °C; from 8 s to 16 s, G = 0.4 Suns and T = 35 °C; from 16 s to 24 s, G = 0.7 Suns and T = 45 °C; from 24 s to 32 s, G = 1.0 Suns and T = 55 °C; and from 32 s to 40 s, G = 0.9 Suns and T = 50 °C. By varying the values of G and T the corresponding variation in the voltage and current of PV array can be observed from subplots (b) and (c) of Fig. 7 respectively. Also, the inverse relationship between PV array voltage and current can be observed in these subplots. From 0 to 32 s, the increasing environmental conditions were considered. At time 32 s, both the insolation and temperature are reduced from 1 Sun to 0.9 Suns and 55 °C to 50 °C respectively. The effect of insolation will be mostly on the PV current and a slight change in the temperature will reflect on the PV voltage. Due to this reason, the PV

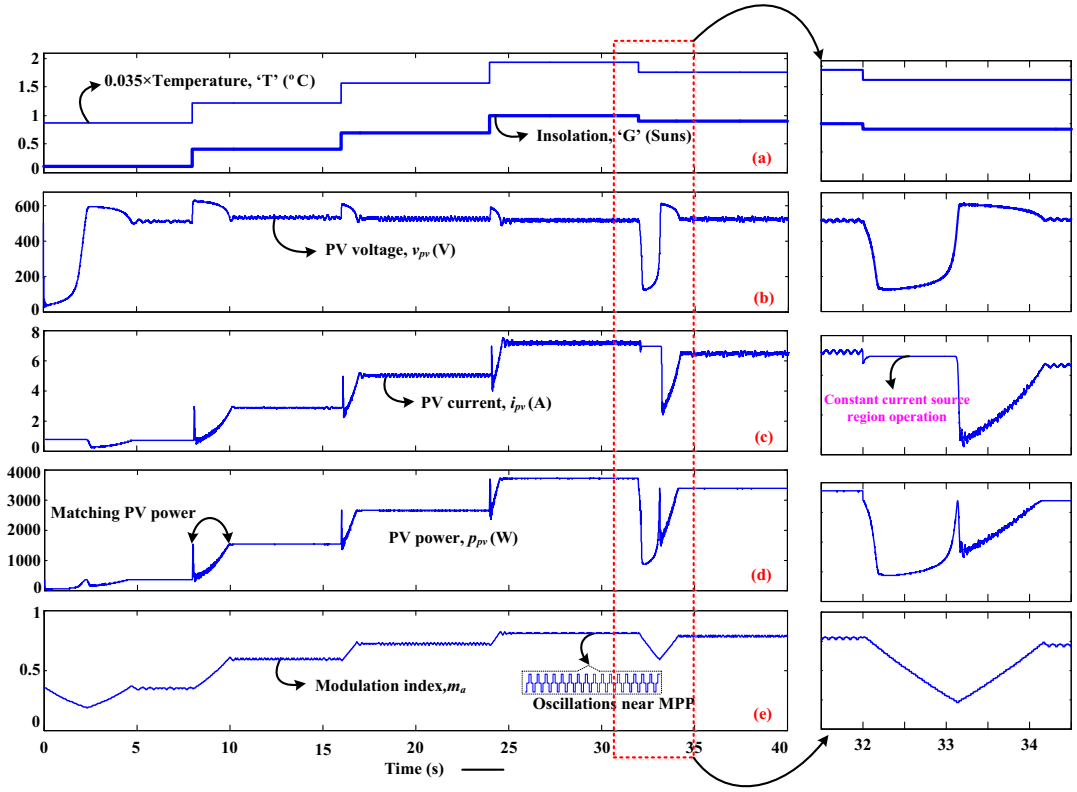

Fig. 7. Simulation results at PV source side.

source enters into current source region i.e., PV current reaches to the value of short circuit current (this can be observed from zoomed part of Fig. 7). Until the PV source entering into the current source region, the inverse relationship between PV voltage and current can be observed. Later, the MPPT algorithm carry the necessary action to bring back the PV source near MPP i.e., the voltage source region. This can be supported by the appearance of a spike in the PV power nearly at 33 s as shown in Fig. 7(d) and its zoomed part.

Another, observation to be noted from Fig. 7 is that the modulation index 'm_a' for three-level cascaded inverter follows the generated PV power. The varying nature of PV power with respect

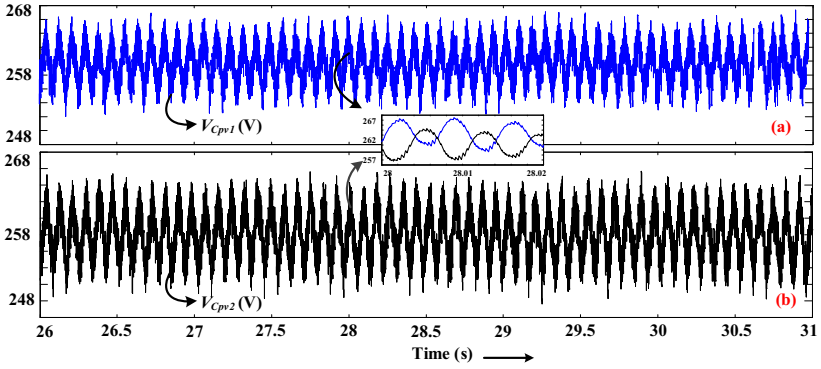

Fig. 8. Voltage across PV/dc-bus capacitors (a) C_{pv1} and (b) C_{pv2}.

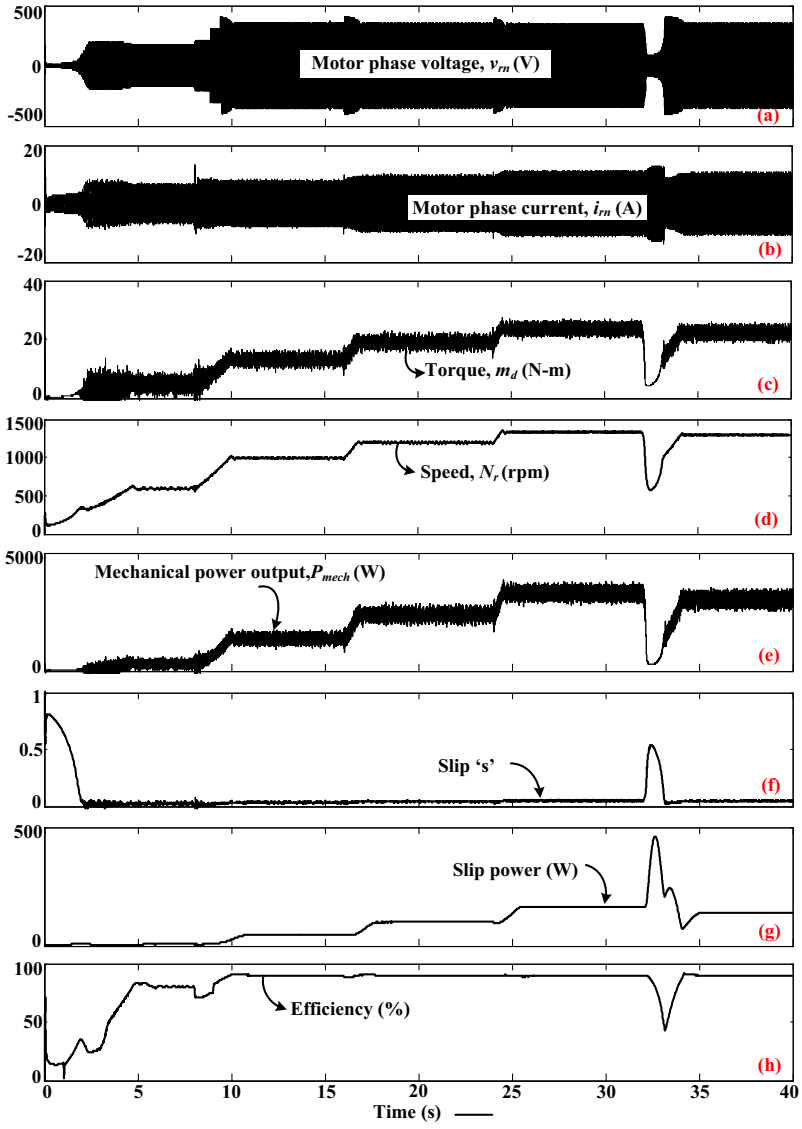

Fig. 9. Simulation results at motor pump side: motor phase voltage, phase current, developed torque, rotor speed, mechanical power output, slip, slip power and efficiency.

to G and T leads to the corresponding variation in the value of 'm_a'. Another important thing to be noted that the operating voltage of solar PV array passes through optimum (MPP) voltage for every step increase in G and T. Also, the small oscillations in 'm_a' (see zoomed part in Fig. 7(e)) value clearly indicates the operation of PV array near MPP. This can also be concluded with the matching values of peak power during transient tracking and steady-state near MPP as given in the PV power subplot (d) of Fig. 7.

In addition, from the subplot (b) of Fig. 7 it can be noted that the PV voltage waveform show a sudden rise or fall in its value during the step increase or decrease respectively in G and T. This can be

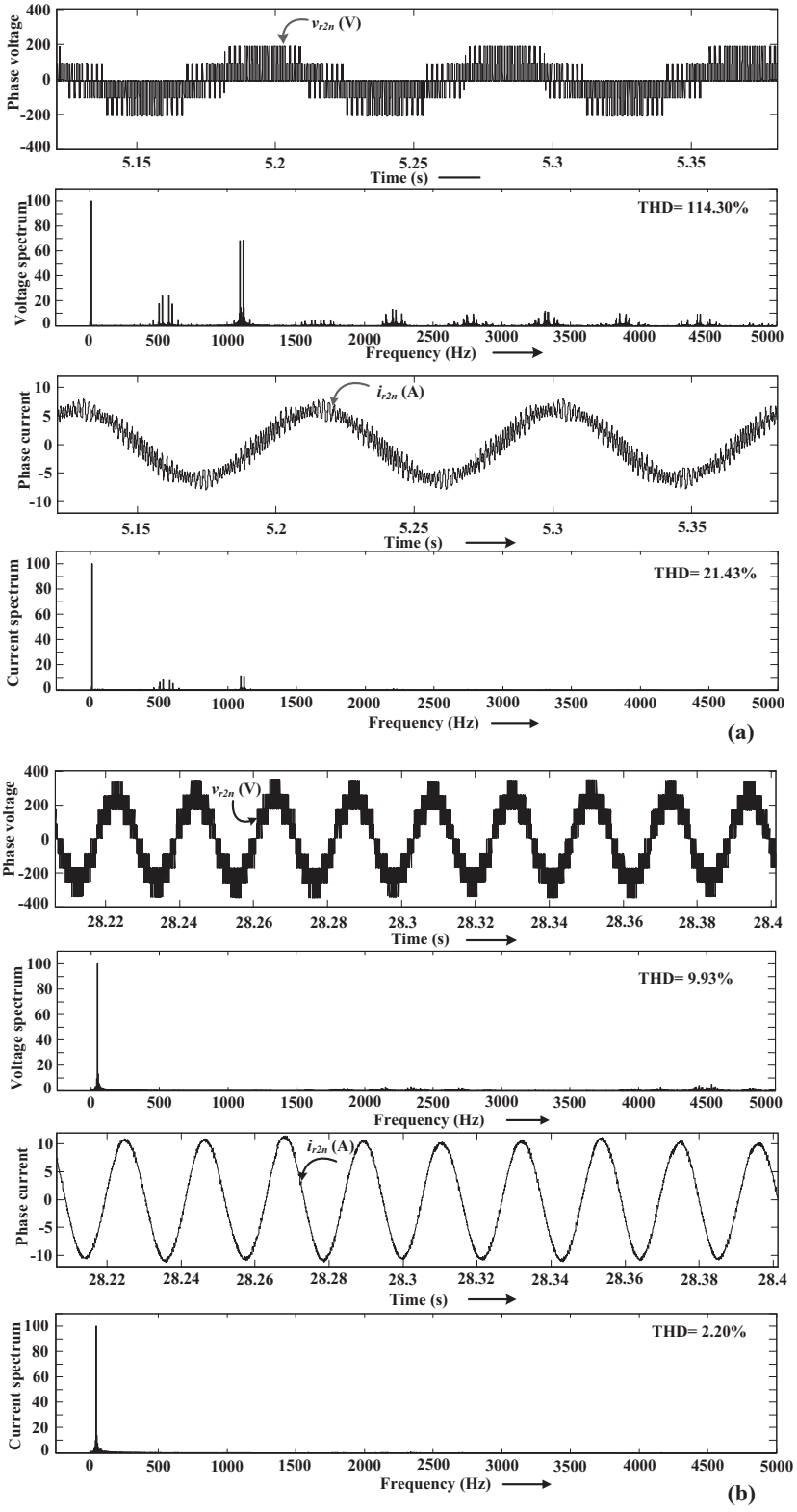

Fig. 10. Motor phase voltage, v_{r2n} and current, i_{r2n} with its FFT plot at steady state (a) for low value and (b) high of modulation index (m_a) respectively.

attributed to the charging and discharging of PV/dc-bus capacitors 'C_{pv1}' and 'C_{pv2}' with excess or deficit PV power during transient condition. Fig. 8 shows the voltage waveform across the PV/dc-bus capacitors C_{pv1} and C_{pv2}. The alternating nature of charging and discharging of the capacitors prove the voltage balancing in the neutral point. This can be observed from the zoomed part of Fig. 8. Also, the low value of ripple content (i.e., about 6 V) in the capacitor voltage confirms the voltage balancing.

Fig. 9 shows the simulation results for motor side parameters like motor phase voltage, phase current, developed torque, rotor speed, mechanical power output, slip and slip power. The variations in PV voltage with respect to G and T can be observed in the peak value of motor phase voltage (see subplot (a)). Also, the motor phase current increases or decreases with the increase or decrease in the value of G and T respectively as shown in subplot (b) of Fig. 9. Further, it can be observed that the developed torque, speed and mechanical power follows the PV power. This can be observed in the subplots (c), (d) and (e) of Fig. 9. Further, the low value of slip and slip power demonstrates the high efficiency as shown in subplots (f), (g) and (h) of Fig. 9 respectively.

Fig. 10(a) and (b) show the expanded view of the motor phase voltage and current waveform from the subplots (a) and (b) of Fig. 9 respectively. High magnitude of ripple content in the voltage and current waveforms at low G and T can be attributed to the lower efficiency as shown in Fig. 9(h). This can be observed from the FFT plots of motor phase voltage and current as shown in Fig. 10(a). Further, the THD of the phase voltage and current improves with the increase in the value of output power. Also, the magnitude of ripple content in the phase current decreases and hence the torque ripple decreases with the increase in output power. Furthermore, the sinusoidal nature of the motor phase current ensures the voltage balance in the dc-bus capacitors [35]. Further, the change in the value of fundamental frequency can be observed for the low and high insolation condition. During low and high insolation value of 'm_a' at steady state is minimum and maximum respectively.

5. Comparison of proposed inverter topology with conventional two-level inverter

To compare PV pumping system performances of three-level inverter operation with the existing two-level inverter another simulation is done and the results are shown in Fig. 11. Fig. 11 (a1) to (d1) are the simulation results for the PV pumping system with two-level inverter; whereas Fig. 11(a2) to (d2) are the results obtained with the three-level cascaded inverter. These results are captured by performing the simulation with three different environmental conditions as given in Table 2. Similar PV array rating and its specifications for the same motor (see Table 1) are considered for both the simulations.

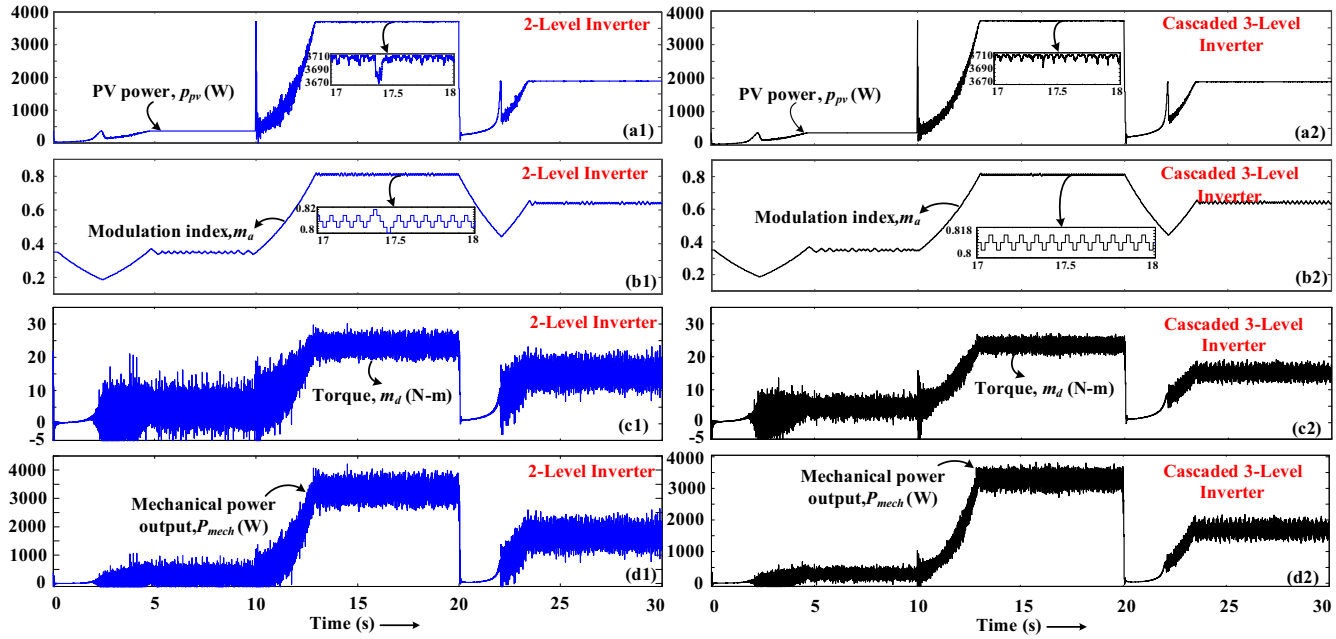

Fig. 11. Simulation results of (top to bottom) PV power, modulation index, torque and mechanical power output of PV pumping system with conventional two-level (left side) and cascaded three-level inverter (right side) respectively.

Table 2
Summary of simulation results for the proposed and the conventional PV pumping systems.

Parameter	Conventional PV pumping system with two-level inverter			Proposed PV pumping system with cascaded three-level inverter		
	G = 0.1 Suns T = 25 °C	G = 0.5 Suns T = 40 °C	G = 1.0 Suns T = 55 °C	G = 0.1 Suns T = 25 °C	G = 0.5 Suns T = 40 °C	G = 1.0 Suns T = 55 °C
PV power ripple (W)	2.3	28	47	1.4	14	37
O/P power ripple (W)	588.9	496	403	246.90	251	265
Torque ripple (N-m)	9.56	4.44	2.88	3.96	2.14	1.9
Voltage THD	93.66	41.33	32.86	41.57	19.84	17.55
Current THD	13.69	5.62	4.14	6.59	2.49	2.09
Flow rate (m^3/Annum)	21,462	126669.6	247,032	21812.4	126844.8	247382.4

The ripple content in the PV power and oscillations in the 'm_a' are higher for the two-level operation when compared to that of three-level as shown in Fig. 11. Higher the oscillations in the value of 'm_a', higher is the ripple content in the PV power. The low ripple content in PV power attributes to effective tracking of maximum power and PV source utilization. The proposed control strategy for three-level cascaded inverter minimizes the oscillations in 'm_a'. This also affects the motor generated torque and the output power. Hence, the ripple content in the torque and the output power is reduced when a three-level cascaded inverter is introduced in the PV pumping system.

The effectiveness of the proposed system and the control strategy can also be observed from Table 2, which is the summary of simulation results shown in Fig. 11. From Table 2, it can be observed that the ripple content in the PV power, motor output power and the motor generated torque is more in case of two-level operation when compared to the three-level operation. Also, the THD values of voltage and current are less in case of three-level operation. So, the ripple content and the THD values may affect the performance of the PV pumping system and reflects in terms of the flow rate as shown in Table 2. Hence, to conclude the use of three-level cascaded inverter in the PV pumping application may give the better performance and the enhanced flow rate output.

6. Experimental results

To emulate or approximate near to PV source characteristics a small value of series resistance is added between programmable dc supply and three-level cascaded inverter input dc terminals as shown in Fig. 12. The programmable dc power supply operating in Constant Voltage (CV) mode with a given value of current limit is used in the experimental set-up. The voltage/current limits for the dc supply are set to 200 V/1.0 A. The power from the dc source *via* the cascaded inverter is fed to a 3-Φ squirrel cage IM with specifications 440 V, 1.5 A, 1440 rpm, 1 HP and is coupled to water pump load. The three-level cascaded inverter is built using 12 IGBT (IXXH30N60B3) switches. Gate pulses required by these switches are generated from dSPACE CP1104 and are given to inverter switches via a driver IC (HCPL3120). The proposed control algorithm is implemented in dSPACE. It includes both, the MPPT algorithm for the source and SVPWM algorithm along with V/*f* control for IM.

For MPP tracking of source, the algorithm requires the information of voltage and current of the emulated PV source. The required information is given by sensing PV voltage with difference amplifier circuit using TL084 Op-Amp IC. And PV current is sensed using the sensor LEM 55-P. The sensed PV voltage and current of source are given to two ADC's of the dSPACE. The computing system internally generates the value of 'm_a' required for the SVPWM algorithm. The given algorithm then generates the required gating signals for Inverter-1 and Inverter-2 (as shown in Fig. 4).

Fig. 13(a) shows the source voltage, current, power and the modulation index captured from the experimental set-up. Increasing value of modulation index and input power confirms the MPP tracking as shown in Fig. 13(a). Oscillations in the modulation index near MPP of the inverter can also be observed. Further, dip in the voltage waveform also confirms MPPT or operation of source at MPP. In addition, the voltage across the dc-bus capacitors is captured and shown in Fig. 13(b). The constant value of capacitor voltage and the lower ripple content in Fig. 13(b) assures the balance between the capacitor voltages.

Fig. 14 shows the experimental results for the parameters at the three-level cascaded inverter output. It shows the phase voltage and current waveform at inverter output terminals with their respective FFT plots. It can be noted that at low and high power operations, the FFT plot of voltage and current waveform indicates harmonic components at same frequency window. Same can be observed in simulation results shown in Fig. 10. Further, the pattern in the waveforms of phase voltage and current is similar to that obtained from simulation results.

Further, to show the effectiveness of the proposed control algorithm for the proposed system, different environmental conditions are considered. These conditions are emulated by changing the current limit of programmable power supply from 0.8 A to 1.3 A and then brought back to 0.8 A with the voltage 175 V. This would

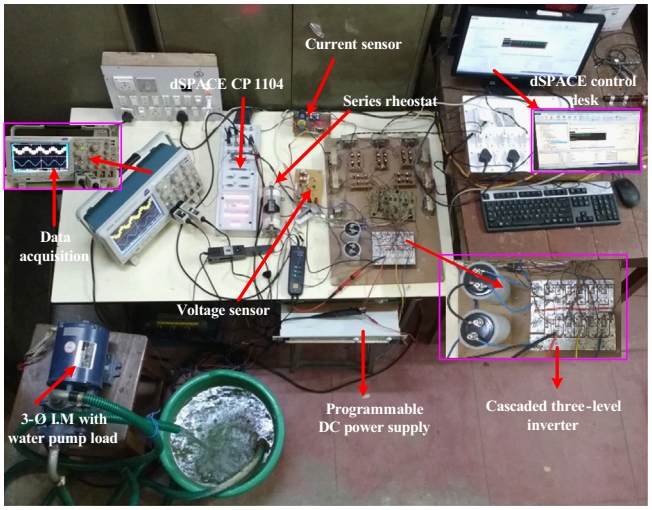

Fig. 12. Experimental prototype setup of the proposed system.

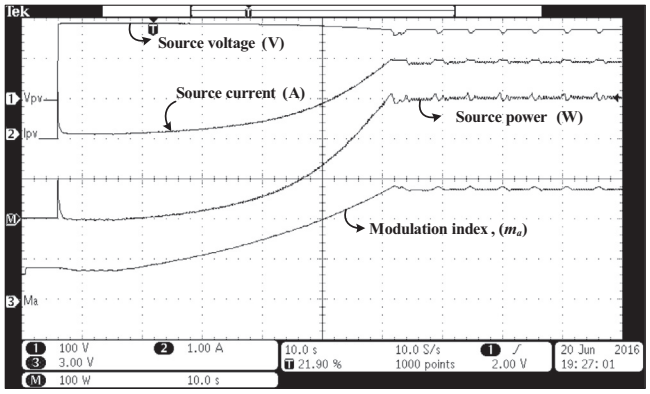

(a)

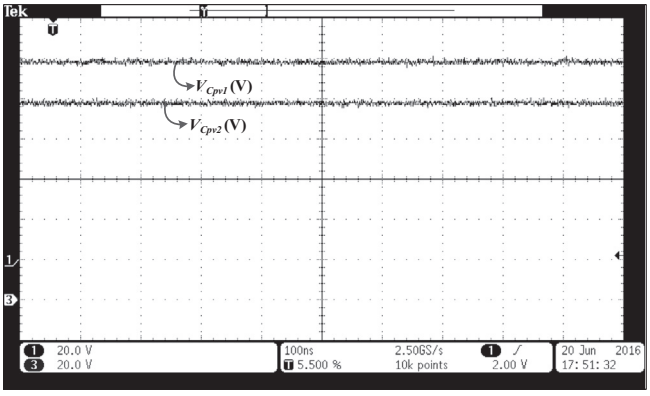

(b)

Fig. 13. Experimental results showing (a) the source voltage, source current and source power with the modulation index, (b) voltages across the dc-bus capacitors.

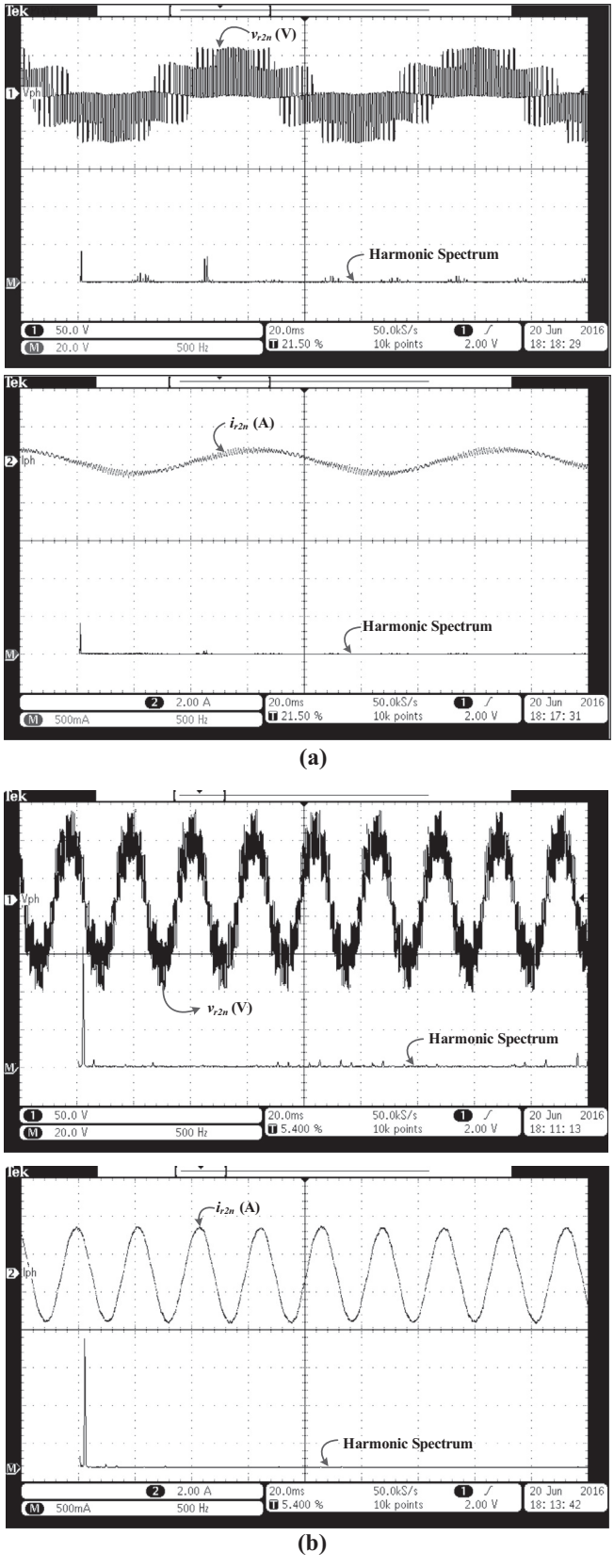

Fig. 14. Experimental results at motor-pump side of the proposed system i.e., Phase voltage (top) and phase current (bottom) of motor and their harmonic spectrum at (a) low power operation and (b) high power operation.

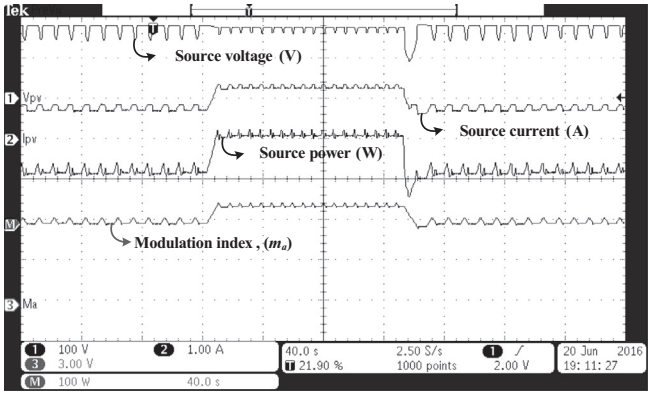

Fig. 15. Experimental result showing important waveforms of PV voltage, current and power with modulation index during different environmental conditions.

nearly emulate the increasing and then decreasing insolation in the PV array system. Fig. 15 show the experimental results for these conditions and the values of set voltage and current can be observed. The results in Fig. 15 show the stable system behavior even under the changing environmental conditions.

7. Conclusions

In this paper, an optimized single-stage solution for three-level cascaded inverter for PV fed pump application is presented. The proposed system is operated using the control strategy which integrates MPPT, SVPWM technique and open-loop V/*f* control. The detailed explanation of the control strategy is presented. Efficient operation of the PV source is justified with operation near MPP both in simulation and experimental results. In addition, a detailed comparison between the PV pumping systems with three-level and two-level inverters is presented. To conclude, the proposed system gives better performance of the PV source as well as the IM with the use of three-level cascaded inverter as presented in this paper.

References

[1] V. Fernão Pires, J.F. Martins, D. Foito, Chen Hão, A grid connected photovoltaic system with a multilevel inverter and a Le-Blanc transformer, Int. J. Renew. Energy Res. 2 (1) (2012).
[2] Le An, Dylan Dah-Chuan Lu, Design of a single-switch DC/DC converter for a PV-battery-powered pump system with PFM + PWM control, IEEE Trans. Industr. Electron. 62 (2) (Feb. 2015) 910–921.
[3] J. Philip et al., Control and implementation of a standalone solar photo-voltaic hybrid system, IEEE Trans. Ind. Appl. 52 (4) (July-Aug. 2016) 3472–3479.
[4] Sachin Jain, Ch. Ramulu, P. Sanjeevikumar, Olorunfemi Ojo, Ahmet H. Ertas, Dual MPPT algorithm for dual PV source fed open-end winding induction motor drive for pumping application, Eng. Sci. Technol.: Int. J. (JESTECH), Elsevier Journal Publications (16 Jul 2016).
[5] M.N. Amrani, A. Bib, Predictive direct power control of a grid connected three-phase voltage source inverter for photovoltaic systems, Int. J. Renew. Energy Res. 6 (1) (2016).
[6] M. Venkatesan, R. Rajeswari, N. Deverajan, A fuzzy logic based three phase inverter with single DC source for grid connected PV system employing three phase transformer, Int. J. Renew. Energy Res. 5 (3) (2015).
[7] Monirul Islam, Saad Mekhilef, H6-type transformerless single-phase inverter for grid-tied photovoltaic system, IET Power Electron. 8 (4) (April 2015) 636–644.
[8] P. Sanjeevikumar, Frede Blaabjerg, Patrick Wheeler, Olorunfemi Ojo, Three-phase multilevel inverter configuration for open-winding high power application, in: Conf. Proc., The 6th IEEE Intl. Symp. on Power Electron. For Distributed Generation Systems, IEEE-PEDG'15, Aachen, Germany, 22–25 Jun. 2015.
[9] P. Sanjeevikumar, Frede Blaabjerg, Patrick Wheeler, Raghav Khanna, S.B. Mahajan, Sanjeet Dwivedi, Optimized carrier based five-level generated modified dual three-phase open-winding inverter for medium power

application, in: Conf. Prof. of IEEE International Transportation Electrification Conf. and Expo, Asia-Pacific, (IEEE-ITEC'16), Busan, Korea, 1–4 Jun. 2016, pp. 40–45.
[10] N.S. Jayalakshmi, D.N. Gaonkar, Pramod Bhat Nempu, Power control of PV/fuel cell/super capacitor hybrid system for stand-alone applications, Int. J. Renew. Energy Res. 6 (2) (2016).
[11] Seif Eddine Boukebbous, Messaoud Khelif, Djallel Kerdoun, Voltage control of standalone photovoltaic system, Int. J. Renew. Energy Res. 4 (3) (2014).
[12] Dipankar Debnath, Kishore Chatterjee, Two-stage solar photovoltaic-based stand-alone scheme having battery as energy storage element for rural deployment, IEEE Trans. Industr. Electron. 62 (7) (July 2015) 4148–4157.
[13] J. Appelbaum, Starting and steady-state characteristics of dc-motors powered by solar cell generators, IEEE Trans. Energy Convers. EC-1 (1) (Mar. 1986) 17–25.
[14] Nadia A. Elsonbaty, Mohamed A. Enany, Mahmoud M. Gamil, Soft computing modelling of a directly coupled PV water pumping system, Int. J. Renew. Energy Res. 6 (1) (2016).
[15] Mukesh Kumar Gupta, Rohit Jain, MPPT simulation with DC submersible solar pump using output sensing direct control method and Cuk converter, Int. J. Renew. Energy Res. 3 (1) (2013).
[16] M.A. Elgendy, B. Zahawi, D.J. Atkinson, et al., Comparison of directly connected and constant voltage controlled photovoltaic pumping systems, IEEE Trans. Sustainable Energy 1 (3) (Oct. 2010) 184–192.
[17] S.M. Alghuwainem, Steady-state performance of DC motors supplied from photovoltaic generators with step-up converter, IEEE Trans. Energy Convers. 7 (2) (1992) 267–272.
[18] S.R. Bhat, A. Pittet, B.S. Sonde, Performance optimization of induction motor-pump system using photovoltaic energy source, IEEE Trans. Ind. Appl. 23 (6) (1987) 995–1000.
[19] Aurobinda Panda, M.K. Pathak, S.P. Srivastava, Solar direct torque controlled induction motor drive for industrial applications, Int. J. Renew. Energy Res. 3 (4) (2013).
[20] Y. Yao, P. Bustamante, R.S. Ramshaw, Improvement of induction motor drive systems supplied by photovoltaic arrays with frequency control, IEEE Trans. Energy Convers. 9 (2) (1994) 256–262.
[21] Mona N. Eskander, Aziza M. Zaki, A maximum efficiency photovoltaic induction motor pump system, Elsevier J. Renew. Energy 10 (1) (1997) 53–60.
[22] M.A. Vitorino, M.B. de Rossiter Corrêa, An effective induction motor control for photovoltaic pumping, IEEE Trans. Industr. Electron. 58 (4) (Apr. 2011) 1162–1170.
[23] G. Grandi, A. Tani, P. Sanjeevikumar, D. Ostojic, Multi-phase multi-level ac motor drive based on four three-phase two-level inverters, in: Conf. Proc. IEEE Intl. 20th Symposium on Power Electron., Elect. Drives etc., IEEE-SPEEDAM'10, Pisa, Italy, 14–16 Jun. 2010, pp. 1768–1775.
[24] P. Sanjeevikumar, G. Grandi, Frede Blaabjer, Patrick Wheeler, Olorunfemi Ojo, Analysis and implementation of power management and control strategy for six-phase multilevel AC drive system in fault condition, Eng. Sci. Technol.: Int. J. (JESTECH), Elsevier Journal Publications 19 (1) (Mar. 2016) 31–39.
[25] G. Grandi, P. Sanjeevikumar, D. Casadei, Preliminary hardware implementation of a six-phase quad-inverter induction motor drive, in: Conf. Proc. The 14th IEEE European Power Electron. Appl., IEEE-EPE'11, Birmingham, United Kingdom, 30 Aug.–1 Sept. 2011, pp. 1–9.
[26] S. Ozdemir, N. Altin, I. Sefa, G. Bal, PV supplied single stage MPPT inverter for induction motor actuated ventilation systems, Elektron. Elektrotech. 20 (5) (Jan. 2014) 116–122.
[27] S. Jain, A.K. Thopukara, R. Karampuri, V.T. Somasekhar, A single-stage photovoltaic system for a dual-inverter-fed open-end winding induction motor drive for pumping applications, IEEE Trans. Power Electron. 30 (9) (Sept. 2015) 4809–4818.
[28] S. Jain, R. Karampuri, V.T. Somasekhar, An integrated control algorithm for a single-stage PV pumping system using an open-end winding induction motor, IEEE Trans. Industr. Electron. 63 (2) (Feb. 2016) 956–965.
[29] P. Sanjeevikumar, Michael Pecht, An isolated/non-isolated novel multilevel inverter configuration for dual three-phase symmetrical/asymmetrical converter, Eng. Sci. Technol.: Int. J. (JESTECH), Elsevier Journal Publications (8 Aug. 2016).
[30] V.T. Somasekhar, K. Gopakumar, Three-level inverter configuration cascading two-level inverters, IEE Proc. Electr. Power Appl. 150 (3) (2003) 245–254.
[31] G. Walker, Evaluating MPPT converter topologies using a MATLAB PV model, J. Electr. Electron. Eng. 21 (1) (2001) 49–56.
[32] Paul Krause, Oleg Wasynczuk, Scott Sudhoff, Steven Pekarek, Analysis of Electric Machinery and Drive Systems, John Willey & Sons, 2013 (Chap. 6).
[33] Mida Dris, Benattous Djilani, Comparative study of algorithms (MPPT) applied to photovoltaic systems, Int. J. Renew. Energy Res. 3 (4) (2013).
[34] Dong Jiang, Fei (Fred) Wang, Variable switching frequency PWM for three-phase converters based on current ripple prediction, IEEE Trans. Power Electron. 28 (11) (Nov. 2013) 4951–4961.
[35] Ja-Hwi Cho, Nam-Joon Ku, Ji-Tai Han, R.Y. Kim, Dong-Seok Hyun, A simple control method for neutral-point voltage oscillation reduction of three-level Neutral-Point-Clamped inverter, in: Industrial Electronics Society, IECON 2013 – 39th Annual Conference of the IEEE, Vienna, 2013, pp. 304–309.